PCCP

PAPER

View Article Online
View Journal | View Issue

Cite this: *Phys. Chem. Chem. Phys.*, 2023, **25**, 26917

Full-dimensional automated potential energy surface development and detailed dynamics for the $CH_2OO + NH_3$ reaction

Cangtao Yin * and Gábor Czakó *

Received 21st July 2023,
Accepted 25th September 2023

DOI: 10.1039/d3cp03469k

rsc.li/pccp

With the help of the ROBOSURFER program package, a global full-dimensional potential energy surface (PES) for the reaction of the Criegee intermediate, CH_2OO, with the NH_3 molecule is developed iteratively using different *ab initio* methods and the monomial symmetrization fitting approach. The final permutationally-invariant analytical PES is constructed based on 23447 geometries and the corresponding ManyHF-based CCSD(T)-F12b/cc-pVTZ-F12 energies. The accuracy of the PES is confirmed by the excellent agreement of its stationary-point properties and one-dimensional potential energy curves compared with the corresponding *ab initio* data. The reaction probabilities and integral cross sections are calculated for the ground-state and several vibrationally excited-state reactions by quasi-classical trajectory simulations. Remarkable is that the maximum impact parameter b where reactivity vanishes is almost independent of collision energy ranging from 1 to 40 kcal mol^{-1}, and the reaction probability increases with increasing collision energy for this negative-barrier reaction. At the same time, a slight mode-specificity effect is observed. In addition, the deuterium effect is investigated and the sudden vector projection is discussed.

I. Introduction

Carbonyl oxides, also called Criegee intermediates, are found to play a significant role in the global atmospheric processes. Due to having C=O–O functional groups, Criegee intermediates are very reactive and they decompose to yield OH radicals[1–5] or react with many atmospheric species such as water,[6,7] sulfur dioxide,[8–11] nitrogen dioxide,[10,11] ammonia,[12–18] methanol,[19–21] organic and inorganic acids.[22–28]

As the most abundant alkaline atmospheric compound, ammonia is believed to play an important role in the formation of inorganic aerosols[29,30] and secondary organic aerosols.[31,32] In regard to the reaction of the simplest Criegee intermediate CH_2OO with NH_3, Misiewicz *et al.*[12] calculated a rate coefficient of 5.36×10^{-14} cm^3 molecule^{-1} s^{-1}. The product of the $CH_2OO + NH_3$ reaction is predicted to be the NH_2CH_2OOH adduct, which may further undergo photolytic breaking of the fragile O–O bond or react with OH radicals. Later Liu *et al.*[13] measured the rate coefficient of the $CH_2OO + NH_3$ reaction with two different experimental methods, the OH laser-induced fluorescence method and the UV transient absorption method. Weak temperature dependence was observed, consistent with the theoretical activation energy of −0.53 kcal mol^{-1} at the QCISD(T)/CBS//B3LYP/6-311+G(2d,2p) level. The rate coefficient was 5.64×10^{-14} cm^3 molecule^{-1} s^{-1} and 8.1×10^{-14} cm^3 molecule^{-1} s^{-1} by both methods at 298 K, within the error bars of the theoretical results. Chhantyal-Pun *et al.*[14] also investigated the $CH_2OO + NH_3$ reaction both theoretically and experimentally. The average rate coefficient was 8.4×10^{-14} cm^3 molecule^{-1} s^{-1} deduced at 293 K. Photoionization mass spectra indicated production of NH_2CH_2OOH functionalized organic hydroperoxide adduct from the reaction. *Ab initio* calculations performed at the CCSD(T)(F12*)/cc-pVQZ-F12//CCSD(T)(F12*)/cc-pVDZ-F12 level of theory predicted pre-reactive complex formation, consistent with previous studies. Master equation simulations of the experimental data using the *ab initio* computed structures identified submerged barrier heights of −0.50 kcal mol^{-1}, similar with the results from Liu *et al.*[12] Adjieufack *et al.*[17] analyzed the flow of the electron density along the $CH_2OO + NH_3$ reaction from the perspective of bonding evolution theory. In addition to the initial adduct NH_2CH_2OOH, four reaction pathways including $CH_2(O)NH_2^{\bullet} + OH^{\bullet}$, $H_2NC(O)H + H_2O$, $H_2CNH + HOOH$ and $H_2CNH + H_2OO$ as afterward products are determined by Nazari and Saheb as possible product channels.[18]

First-principles dynamics investigations of the $CH_2OO + NH_3 \rightarrow NH_2CH_2OOH$ reaction have been hindered, because

MTA-SZTE Lendület Computational Reaction Dynamics Research Group, Interdisciplinary Excellence Centre and Department of Physical Chemistry and Materials Science, Institute of Chemistry, University of Szeged, Rerrich Béla tér 1, Szeged H-6720, Hungary. E-mail: cangtaoyin@foxmail.com, gczako@chem.u-szeged.hu

no potential energy surface (PES) is available in the literature. The only full-dimensional PES related to Criegee intermediates we can find is for the $CH_2OO + H_2O$ reaction, reported by Wu *et al.*[33] very recently, which was developed based on high-level CCSD(T)-F12a/aug-cc-pVTZ data. Extensive quasi-classical trajectory (QCT) calculations were performed on that PES providing detailed kinetics and dynamics results. In this research, we develop a full-dimensional *ab initio* PES for the $CH_2OO + NH_3 \rightarrow NH_2CH_2OOH$ reaction. Next, the QCT simulations are carried out on this PES. In addition, the normal-mode excitations and the deuterium effect are also investigated.

II. PES

A. Initial PES

Following our previous approach for the HBr/HI + C_2H_5 reactions,[34,35] first we randomly displace the Cartesian coordinates[13] of the vdW complex, the transition state, and the product of the $CH_2OO + NH_3 \rightarrow NH_2CH_2OOH$ reaction in the 0 Å–0.4 Å interval, resulting in 1000 geometries for each stationary point. For the entrance region, the distance between CH_2OO and NH_3 is randomly set between 3 and 8 Å, which generated 2000 geometries. Next the energies of these geometries at the ManyHF-based[36] MP2[37]/aug-cc-pVDZ[38] level of theory are calculated using the MOLPRO program package[39] as our initial candidate of geometry set. It should be noticed that for the geometries far from equilibrium, the Hartree–Fock (HF) method offers no guarantee to find the lowest-energy solution even if convergence is achieved. Therefore, in this work we use the ManyHF method recently developed in our group,[36] which finds better HF solutions. Since geometries with too high energy are not needed in the global PES and could even damage the analytical PES, we exclude those geometries with energies higher than 400 kcal mol^{-1} relative to the global minimum of the set, which is the stationary point of the product in this case. Now we have a dataset consisting of 4557 geometries and the corresponding energies in hand.

To get an initial full-dimensional analytical PES function the Monomial Symmetrization Approach (MSA)[40] is used with the above data set. This function is an expansion of polynomials of the $y_{ij} = \exp(-r_{ij}/a)$ variables, where r_{ij} are the distances between two atoms and the non-linear parameter a is set to 2.0 bohr as we chose before in other systems.[34,35] The method of weighted least squares is used for the fitting, with a weighting factor of $E_0/(E + E_0)$, where E is the potential energy relative to the global minimum, and E_0 is set to 0.1 (in hartree). There are 2121/11241 fitting coefficients in the fourth/fifth-order expansion. Since we have 4557 initial data points, we employed the fourth-order expansion at first.

B. PES development

First round. Our group have developed the ROBOSURFER program package[41] which consists of mainly five parts: (1) determines the analytical PES function (fourth-order) using MSA in the present case and the geometry set; (2) generates the new geometries by monitoring the QCTs[42] on the analytical PES function; (3) selects the most promising geometries from the newly generated geometries; (4) calculates the *ab initio* potential energies using the MOLPRO program package; (5) adds geometries and the corresponding energies that pass all checks (details in ref. 41, for example, any geometries with 400 kcal mol^{-1} more energy than the free reactants are discarded to avoid needless geometries). After that the new analytical PES function can be determined and the iteration continues, thus improving the PES. The ManyHF-based MP2/aug-cc-pVDZ level of theory, same as in section II. A, is used in this round. The collision energy in the QCT computations is set from 1, 10, 20, 30, 40 to 50 kcal mol^{-1}. We increase the collision energy when the percentage of the unphysical trajectories is less than 1%. After 137 iterations we have a PES consisting of 12875 geometries and the corresponding energies.

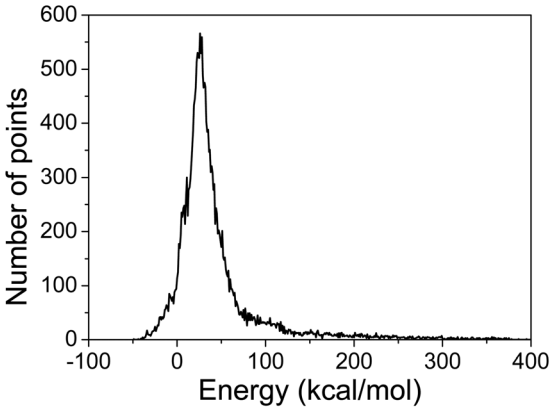

Fig. 1 Distribution of the data points for the final PES. The energy zero point is set at the asymptote of reactants. The bin size is 1 kcal mol^{-1}.

Second round. With the 12875 data set, we can then move to the fifth-order expansion. The rest is same as the first round, just for the sake of time saving, in this round we start the collision energy as 10 kcal mol^{-1} instead of 1 kcal mol^{-1}, and increase it with a step size of 10 kcal mol^{-1} till it reaches 50 kcal mol^{-1}. This round went through 150 iterations and the data set consists of 22456 geometries and the corresponding energies.

Third (final) round. At this stage we can move on to a higher level of theory for the *ab initial* energies. We choose ManyHF-CCSD(T)-F12b/cc-pVTZ-F12 considering both efficiency and accuracy. In the recalculation only 53 points failed in CCSD iteration. Then the third round of iteration is launched. Lucky for us in this round only 13 iterations are needed since the percentage of the unphysical trajectories is already negligible. The final PES is built from 23447 geometries and the corresponding coupled-cluster energies, whose distribution is shown in Fig. 1. We also checked that among these geometries, only 4% have T_1-diagnostic values[43] higher than 0.045. Thus, it is safe to use the single-reference CCSD(T)-F12b method. The root-mean-square (RMS) errors of the PES are 1.06, 1.35, and 2.02 kcal mol^{-1} in the energy intervals of 0–50, 50–100, 100–200 kcal mol^{-1} relative to the global minimum, respectively.

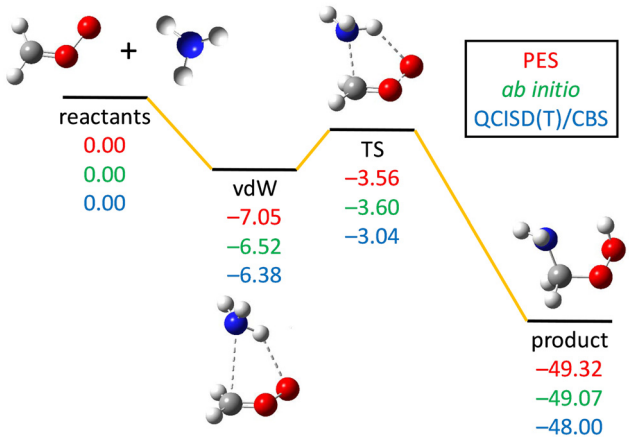

Fig. 2 PES schematic of the $CH_2OO + NH_3 \rightarrow NH_2CH_2OOH$ reaction. All energies are in kcal mol^{-1} and relative to the $CH_2OO + NH_3$ asymptote at three different methods: obtained on the PES (red), the ManyHF-CCSD(T)-F12b/cc-pVTZ-F12 *ab initio* energies at geometries optimized on the PES (green), and the QCISD(T)/CBS relative energies taken from ref. 13 (blue).

C. PES evaluation and test

Fig. 2 shows the reactants, vdW complex, transition state, and the product of the $CH_2OO + NH_3$ reaction. Both the geometry and energy indicate a reactant-like TS. The energies obtained by three different methods (see the caption of Fig. 2) are in good agreement with each other, indicating low fitting errors of the analytical PES function and the fact that reliable results can be deduced from this PES.

The imaginary frequency of the TS is 288*i* cm^{-1} on the PES, which is consistent with the *ab initio* calculations of 302*i* cm^{-1} (Misiewicz *et al.*[12]), 239*i* cm^{-1} (Liu *et at.*[13]), 268*i* cm^{-1} (Chhantyal-Pun *et al.*[14]), and 355*i* cm^{-1} (Nazari and Saheb[18]). The zero-point energies (ZPEs) of CH_2OO, NH_3, vdW complex, transition state, and product obtained on the present PES are 19.32 (19.54), 21.99 (21.54), 43.49 (42.83), 44.49 (43.92), and 46.70 (45.82) kcal mol^{-1}, respectively (the *ab initio* values[13] are listed in parentheses).

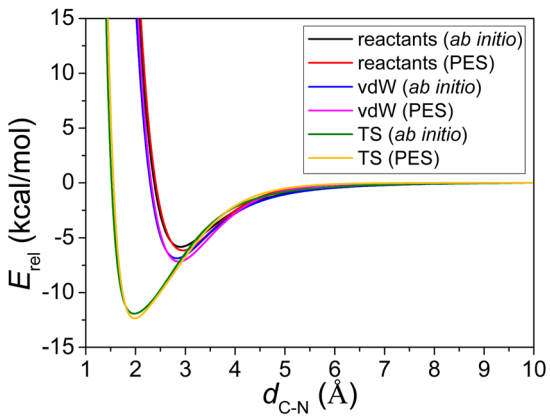

Fig. 3 Comparisons of potential energies as a function of d_{C-N} (distance between the C atom of CH_2OO and the N atom of NH_3) obtained from the PES and from ManyHF-CCSD(T)-F12b/cc-pVTZ-F12 *ab initio* calculations, while fixing all the other internal coordinates for the three situations.

Table 1 The PES (*ab initio*) energies and C–N distances of the wells of the 1D-scans shown in Fig. 3

	Reactants	vdW complex	Transition state
Energy (kcal mol^{-1})	−6.1 (−5.8)	−7.2 (−6.9)	−12.3 (−11.9)
C–N distance (Å)	2.95 (2.90)	2.87 (2.83)	1.98 (1.97)

As shown in Fig. 3, three different potential energy curves are plotted: (1) the optimized reactants, CH_2OO and NH_3, are separated at the distance of 1 Å to 10 Å, in terms of C–N distance; (2) the C–N bond of optimized vdW complex geometry is elongated and shortened, while other degrees of the two parts are frozen; (3) the C–N bond of optimized transition state geometry is elongated and shortened, while other degrees of the two parts are frozen. Note that each curve uses different asymptote in Fig. 3.

The energies of the wells with respect to the corresponding asymptote for the three situations described above are shown in Table 1. The comparison between the PES minima and *ab initio* minima shows a perfect chemical accuracy for this full-dimensional PES and its fitting errors are merely about 0.4 kcal mol^{-1}. Table 1 also offers the positions of the minima located at the C–N distance for PES and *ab initio* (with less than 0.05 Å differences), and they show a good behavior of the analytical PES in the entrance channel.

III. QCT simulations

A common approach used to study the dynamics of chemical reactions is the QCT method, which is computationally easier and faster than quantum methods. In the QCT method, the motion of atoms during the collision is described by classical mechanics. The QCT method has another advantage that it provides the possibility of visualization of the motion of atoms. Thus, one can get insight into the dynamics of the reaction by analyzing the motion of atoms during collisions.

In this paper, the quasi-classical dynamics is carried out based on standard QCT simulations. Seven different collision energies E_{coll} = 1, 2, 5, 10, 20, 30, and 40 kcal mol^{-1} are adopted as one of the initial conditions of the QCT simulations. Other initial conditions include: (1) the ZPEs of the reactants CH_2OO and NH_3 are set by standard normal-mode sampling;[42] (2) the rotational angular momentum of each reactant is set to zero; (3) the spatial orientations of both reactants are randomly sampled; (4) the X/Y/Z-direction distance between the center of mass of the two reactants CH_2OO and NH_3 is set to 16/b/0 bohr, where the center of mass velocities are parallel with the X axis and the impact parameter b takes a value from 0 to b_{max} (no reaction occurs), increasing by 0.5 bohr each time. Two thousand trajectories for each b value are performed to get statistically accurate results. During the simulations, we choose 0.0726 fs as the time step for trajectory propagation. In this cycloaddition reaction, the two reactants collide after around 10 000 time steps. The product is formed around 20 000 time steps if reaction occurs. We set 100 000 time steps for each trajectory and we also stop the propagation when the largest

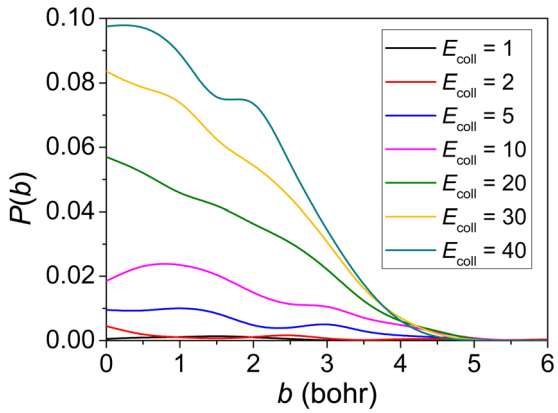

Fig. 4 Reaction probabilities calculated with the QCT method at varying collision energies (given in kcal mol^{-1}).

interatomic distance becomes larger than the largest initial one by 1 bohr. In this case reactive trajectories can stay in the product region long enough and the non-reactive trajectories are halted much earlier to save time. There are of course other ways of defining the reactive event and stopping condition, for example, in the N_2O + C_2H_2 reaction, the trajectories were halted when the distances of the two forming bonds C–N and C–O arrived at 1.6 Å.[44] At the end less than 0.1% of the trajectories failed and gave unphysical results, which also indicates a good behavior of the newly-developed analytical PES.

A. Reaction probabilities

Reaction probabilities of the ground-state reactants corresponding to seven different collision energies are plotted as a function of the impact parameter b in Fig. 4. Remarkable is that the reaction probability increases with increasing E_{coll} for this negative barrier reaction. The reaction probabilities for collision energy as small as 1 kcal mol^{-1} are not zero which means no threshold energy for the CH_2OO + NH_3 → NH_2CH_2OOH reaction. By checking the non-reactive trajectories, we found that sometimes the two reactants rotate with each other, after a few rounds they separate and no reaction occurs. This often happens at low E_{coll}. The maximum b where reactivity vanishes is around 5 bohr and almost independent of E_{coll}.

B. The role of the vibrational excitations and deuterium effect

Comparing how efficiently translational and vibrational energy promote a reaction is popular. By checking the geometries of the reactants and product, we see that the CH_2 is bent down after the reaction, the O–O bond and C–O bond are elongated around 0.11 Å and 0.14 Å, respectively, and also the NH_3 becomes flatter. In addition, the reaction involves N–H bond breaking, as well as C–N bond and O–H bond forming. Clearly the NH-stretching excitation is expected to promote the reaction, so does the translational energy (which has already been proved by Fig. 4). Therefore, we pick the CH_2 wagging, OO-stretching, CO-stretching, NH_3-umbrella-wagging, NH-symmetric-stretching, and NH-asymmetric-stretching normal modes and investigate their efficiency for the reactivity. The motions corresponding to above vibrations are represented in Fig. 5.

In Fig. 6, following the same strategy as before,[45,46] we present the reaction cross sections (σ) obtained with the QCT method for the reaction with both reactants in vibrational ground state as well as for six excited vibrational states described above. The results reflect a slight increment for $v_{OO\text{-}str}$ = 1 and $v_{NH\text{-}str}$ = 1 with both symmetric and asymmetric case, but a slight inhibition effect for $v_{CO\text{-}str}$ = 1 and $v_{CH_2\text{-}wag}$ = 1. However, the excitation of the umbrella mode of NH_3 has the negative effect to the reactivity at low E_{coll} while enhances the reactivity at high E_{coll}.

The deuterium effect by changing NH_3 to ND_3 is also shown in Fig. 6. Despite its usefulness, due to its classical nature, the QCT method does not treat tunneling effect and only the mass is different for H and D, as well as the corresponding ZPEs. As expected the reactivity of ND_3 is weaker (about 20%) compared to NH_3.

Additional information is provided by the sudden vector projection (SVP) model developed by Jiang and Guo.[47,48] The idea beyond this model is the evaluation of the overlaps of the vibrational modes of the reactants with the reaction coordinate (imaginary mode) at TS structure. This is accomplished by

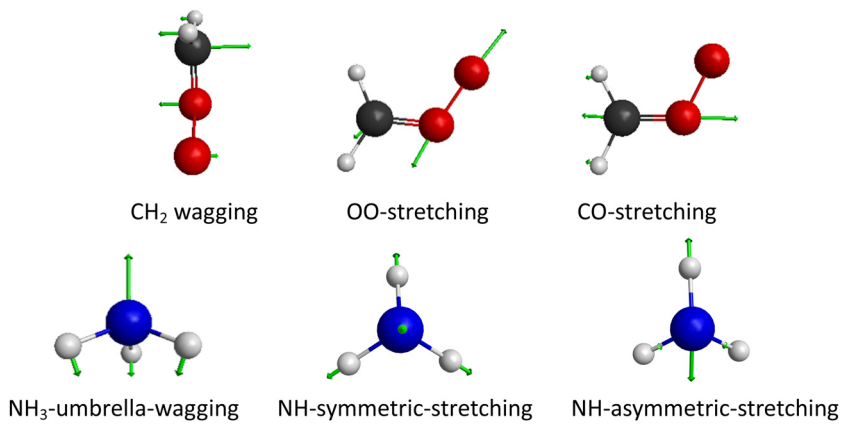

Fig. 5 Six normal-mode vibrations studied in the present work. The normal-mode analysis is performed on the PES.

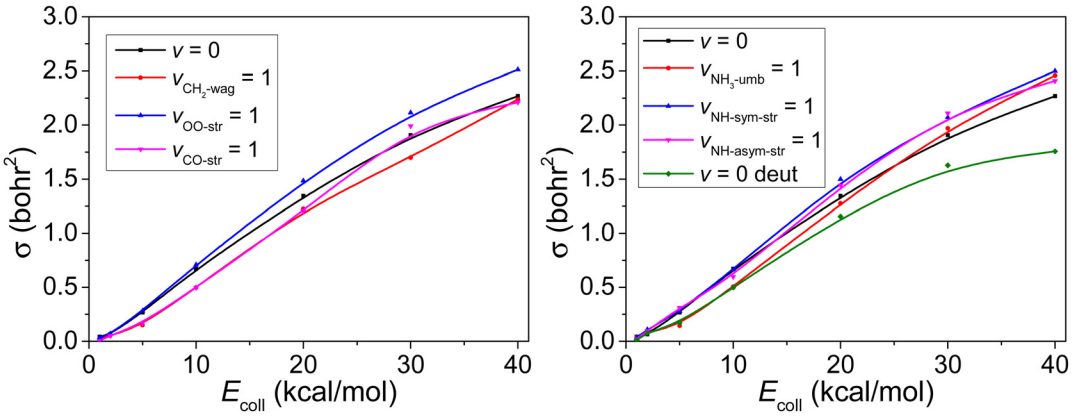

Fig. 6 Integral cross sections as a function of the collision energy for the CH_2OO (v_x = 1) [x = CH_2-wag, OO-str, CO-str] + NH_3 (v = 0) (left panel) and CH_2OO (v = 0) + NH_3 (v_y = 1) [y = NH_3-umb, NH-sym-str, NH-asym-str] (right panel) reactions. The ground-state reaction case (v = 0) is shown in both panels for comparison. In addition, cross sections of the CH_2OO (v = 0) + ND_3 (v = 0) reaction are shown in the right panel, denoted as v = 0 deut.

Table 2 Single-excited vibrational energies and SVP values of the six vibrational normal modes (and translation) for the CH_2OO + NH_3 reaction calculated at the CCSD(T)/cc-pVDZ level of theory, along with the promotion(+)/inhibition(−) effects in terms of integral cross section proportions compared to the ground-state reaction based on QCT results, averaged from seven collision energies

Normal mode	Energy (kcal mol^{-1})	SVP value	QCT
CH_2 wag	2.17	0.247	−10%
OO-str	2.77	0.084	+10%
CO-str	3.62	0.007	−7%
NH_3-umb	3.39	0.113	−1%
NH-sym-str	9.81	0.016	+9%
NH-asym-str	10.17	0.031	+6%
Translation		0.818	

calculating SVP values using the CCSD(T)/cc-pVDZ optimized geometries and the corresponding normal-mode vectors of the TS while the two reactants are placed far. The results are listed in Table 2.

As expect only the translational enhancement is consistent with the prediction of the SVP model, since the imaginary frequency of the TS in the CH_2OO + NH_3 → NH_2CH_2OOH reaction is only 288i cm^{-1}, which could not represent the whole process of reaction very well. Comparing the SVP values and the QCT results we can see that indeed the SVP model failed to predict the vibrational enhancement in this reaction. And only a minor mode-specificity (within 10% based on the QCT results) is seen for the selected vibrational mode excitations.

IV. Conclusions

A full-dimensional PES for the CH_2OO + NH_3 → NH_2CH_2OOH reaction under the framework of the ROBOSURFER program package is developed and its dynamics are presented in detail by performing QCT simulations. The vdW complex, the TS, and the three 1D scans obtained on the PES agree well with the *ab initio* results. QCT simulations on this PES in a wide range of E_{coll} are performed and no threshold energy is found for the CH_2OO + NH_3 → NH_2CH_2OOH reaction, which is expected due to the submerged-barrier, exothermic nature of the system. What unexpected is that the reaction probability increases with increasing collision energy for this negative-barrier reaction. As for the vibrational mode-specificity, a slight enhancement occurs for $v_{OO\text{-}str}$ = 1 and $v_{NH\text{-}str}$ = 1 with both the symmetric and asymmetric case, but a slight inhibition effect for $v_{CO\text{-}str}$ = 1 and $v_{CH_2\text{-}wag}$ = 1 is observed. Interestingly, the excitation of the umbrella mode of NH_3 has a negative effect to the reactivity at low E_{coll} while enhances the reactivity at high E_{coll}. The deuterium effect is also investigated by changing NH_3 to ND_3 and, as expected, the reactivity of ND_3 is weaker compared to NH_3. Only the translational enhancement is consistent with the prediction of the SVP model. The QCT calculations provide useful information on the microscopic mechanism of the reaction. At very low collision energies sometimes the two reactants rotate with each other, and after a few rounds they separate and no reaction occurs.

Data availability

The data that support the findings of this study are available from the corresponding authors upon reasonable request.

Conflicts of interest

There are no conflicts to declare.

Acknowledgements

We thank Tibor Győri and Viktor Tajti for the tips and discussions. This work was supported by the National Research, Development and Innovation Office–NKFIH, K-125317; Project no. TKP2021-NVA-19, provided by the Ministry of Innovation and Technology of Hungary from the National Research, Development and Innovation Fund, financed under the TKP2021-NVA funding scheme; and the Momentum (Lendület) Program of the Hungarian Academy of Sciences.

References

1 A. M. Green, V. P. Barber, Y. Fang, S. J. Klippenstein and M. I. Lester, *Proc. Natl. Acad. Sci. U. S. A.*, 2017, **114**, 12372.
2 C. Yin and K. Takahashi, *Phys. Chem. Chem. Phys.*, 2017, **19**, 12075.
3 B. Long, J. L. Bao and D. G. Truhlar, *Nat. Commun.*, 2019, **10**, 2003.
4 X. Zhou, Y. Liu, W. Dong and X. Yang, *J. Phys. Chem. Lett.*, 2019, **10**, 4817.
5 C. Robinson, L. Onel, J. Newman, R. Lade, K. Au, L. Sheps, D. E. Heard, P. W. Seakins, M. A. Blitz and D. Stone, *J. Phys. Chem. A*, 2022, **126**, 6984.
6 C. Yin and K. Takahashi, *Phys. Chem. Chem. Phys.*, 2018, **20**, 20217.
7 Y. H. Lin, C. Yin, K. Takahashi and J. J.-M. Lin, *Commun. Chem.*, 2021, **4**, 12.
8 C. M. Stangl, J. M. Krasnomowitz, M. J. Apsokardu, L. Tiszenkel, Q. Ouyang, S. Lee and M. V. Johnston, *J. Geophys. Res.: Atmos.*, 2019, **124**, 4800.
9 M. Yang, S. S. Ma, H. Ashraf, S. F. Pang and Y. H. Zhang, *Atmos. Environ.*, 2020, **231**, 117560.
10 O. Welz, J. D. Savee, D. L. Osborn, S. S. Vasu, C. J. Percival, D. E. Shallcross and C. A. Taatjes, *Science*, 2012, **335**, 204.
11 C. A. Taatjes, O. Welz, A. J. Eskola, J. D. Savee, A. M. Scheer, D. E. Shallcross, B. Rotavera, E. P. F. Lee, J. M. Dyke, D. K. W. Mok, D. L. Osborn and C. J. Percival, *Science*, 2013, **340**, 177.
12 J. P. Misiewicz, S. N. Elliott, K. B. Moore and H. F. Schaefer, *Phys. Chem. Chem. Phys.*, 2018, **20**, 7479.
13 Y. Liu, C. Yin, M. C. Smith, S. Liu, M. Chen, X. Zhou, C. Xiao, D. Dai, J. J.-M. Lin, K. Takahashi, W. Dong and X. Yang, *Phys. Chem. Chem. Phys.*, 2018, **20**, 29669.
14 R. Chhantyal-Pun, R. J. Shannon, D. P. Tew, R. L. Caravan, M. Duchi, C. Wong, A. Ingham, C. Feldman, M. R. McGillen and M. A. H. Khan, *et al.*, *Phys. Chem. Chem. Phys.*, 2019, **21**, 14042.
15 W. Chao, C. Yin, K. Takahashi and J. J.-M. Lin, *Phys. Chem. Chem. Phys.*, 2019, **21**, 22589.
16 W. Chao, C. Yin, Y. L. Li, K. Takahashi and J. J.-M. Lin, *J. Phys. Chem. A*, 2019, **123**, 1337.
17 A. I. Adjieufack, M. M. Bake, C. N. Nguimkeu, J. Pilmé and I. M. Ndassa, *Chem. Phys. Chem.*, 2021, **22**, 1792.
18 A. Nazari and V. Saheb, *Theor. Chem. Acc.*, 2022, **141**, 66.
19 Y.-H. Lin, C. Yin, W.-H. Lin, Y.-L. Li, K. Takahashi and J. J.-M. Lin, *J. Phys. Chem. Lett.*, 2018, **9**, 7040.
20 W. Chao, Y.-H. Lin, C. Yin, W.-H. Lin, K. Takahashi and J. J.-M. Lin, *Phys. Chem. Chem. Phys.*, 2019, **21**, 13633.
21 B. Tang and Z. Li, *J. Phys. Chem. A*, 2020, **124**, 8585.
22 O. Welz, A. J. Eskola, L. Sheps, B. Rotavera, J. D. Savee, A. M. Scheer, D. L. Osborn, D. Lowe, A. M. Booth and P. Xiao, *et al.*, *Angew. Chem., Int. Ed.*, 2014, **53**, 4547.
23 E. S. Foreman, K. M. Kapnas and C. Murray, *Angew. Chem., Int. Ed.*, 2016, **55**, 10419.
24 A. Kumar, S. Mallick and P. Kumar, *Phys. Chem. Chem. Phys.*, 2022, **24**, 7458.
25 V. J. Esposito, T. A. McHenry and M. I. Lester, *Chem. Phys. Lett.*, 2022, **809**, 140179.
26 C. A. Chung, C. W. Hsu and Y. P. Lee, *J. Phys. Chem. A*, 2022, **126**, 5738.
27 R. Reynolds, M. Ahmed and K. R. Wilson, *ACS Earth Space Chem.*, 2023, **7**, 901.
28 P. L. Luo, *Phys. Chem. Chem. Phys.*, 2023, **25**, 4062.
29 B. H. Baek, V. P. Aneja and Q. Tong, *Environ. Pollut.*, 2004, **129**, 89.
30 J. L. Hand, B. A. Schichtel, M. Pitchford, W. C. Malm and N. H. Frank, *J. Geophys. Res.: Atmos.*, 2012, **117**, D05209.
31 S. M. Murphy, A. Sorooshian, J. H. Kroll, N. L. Ng, P. Chhabra, C. Tong, J. D. Surratt, E. Knipping, R. C. Flagan and J. H. Seinfeld, *Atmos. Chem. Phys.*, 2007, **7**, 2313.
32 X. Ge, A. S. Wexler and S. L. Clegg, *Atmos. Environ.*, 2011, **45**, 524.
33 H. Wu, Y. Fu, W. Dong, B. Fu and D. H. Zhang, *RSC Adv.*, 2023, **13**, 13397.
34 C. Yin, V. Tajti and G. Czakó, *Phys. Chem. Chem. Phys.*, 2022, **24**, 24784.
35 C. Yin and G. Czakó, *Phys. Chem. Chem. Phys.*, 2022, **24**, 29084.
36 T. Győri and G. Czakó, *J. Chem. Phys.*, 2022, **156**, 071101.
37 C. Møller and M. S. Plesset, *Phys. Rev.*, 1934, **46**, 618.
38 T. H. Dunning Jr., *J. Chem. Phys.*, 1989, **90**, 1007.
39 H.-J. Werner, P. J. Knowles, G. Knizia, F. R. Manby, M. Schütz, *et al.*, *Molpro, version 2015.1, a package of ab initio programs*, see **https://www.molpro.net**.
40 Z. Xie and J. M. Bowman, *J. Chem. Theory Comput.*, 2010, **6**, 26.
41 T. Győri and G. Czakó, *J. Chem. Theory Comput.*, 2020, **16**, 51.
42 W. L. Hase, *Encyclopedia of Computational Chemistry*, Wiley, New York, 1998, pp. 399–407.
43 T. J. Lee and P. R. Taylor, *Int. J. Quantum Chem.*, 1989, **36**, 199.
44 Y. Liu and J. Li, *ACS Omega*, 2020, **5**, 23343.
45 C. Yin and G. Czakó, *Phys. Chem. Chem. Phys.*, 2023, **25**, 3083.
46 C. Yin and G. Czakó, *Phys. Chem. Chem. Phys.*, 2023, **25**, 9944.
47 B. Jiang and H. Guo, *J. Chem. Phys.*, 2013, **138**, 234104.
48 H. Guo and B. Jiang, *Acc. Chem. Res.*, 2014, **47**, 3679.